Defect Engineering and Opening of the Ion tracks in the Swift Heavy Ion Irradiated Thin Films of Bismuth Vanadate: Impact on Oxygen Evolution Reaction for Solar Water Splitting

Marko Jelić[a], Zoran Jovanović[a], Ekaterina Korneeva[b], Nina Daneu[c], Suraj Gupta[c], Jacques O'Connell[d], Tatiana Vershinina[be], Nikita Kirilkin[b], Oleg Orelovich[b], Ivana Stojković Simatović[f], Vladimir Skuratov[beg], Sonja Jovanović[a1]

[a]Vinča Institute of Nuclear Sciences – National Institute of the Republic of Serbia, University of Belgrade, Mike Petrovića Alasa 12-14, Belgrade, Serbia [b]Joint Institute for Nuclear Research, Joliot-Curie St.6, Dubna, Russia [c]Jožef Stefan Institute, Jamova 39, Ljubljana, Slovenia

[d]Nelson Mandela University, Summerstrand 6031, Port Elizabeth, South Africa [e]National Research Nuclear University MEPhI, Kashirskoe Shosse, 31, 115409, Moscow, Russia [f]University of Belgrade – Faculty of Physical Chemistry, Studentski trg 12-16, Belgrade, Serbia

[g]Dubna State University, Universitetskaya St., 19, 141982, Dubna, Russia

- Supporting information -

[1] Corresponding author. E-mail: sonja.jovanovic@vin.bg.ac.rs (S. Jovanović)

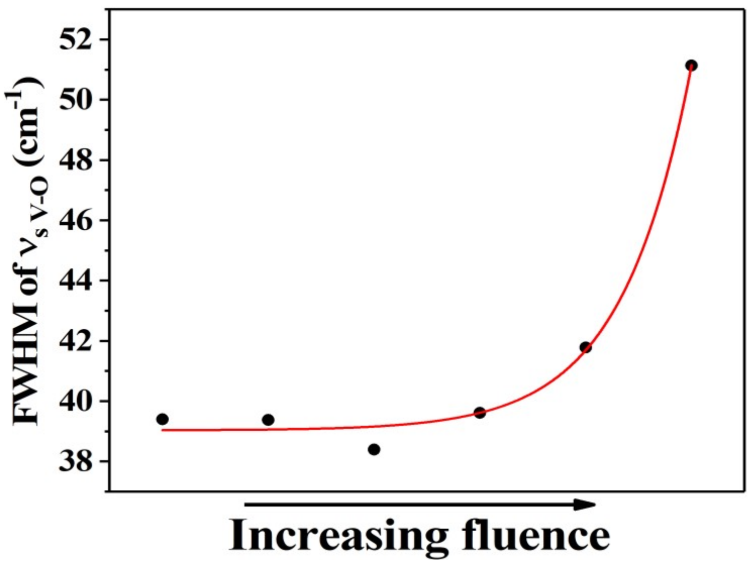

Fig. S1. Change in FWHM of symmetric stretching V-O band with increasing fluence. The first point to the left represents pristine BVO, and going further to the right points represent samples irradiated with $5 \times 10^9 - 5 \times 10^{11}$ ions cm^{-2}.

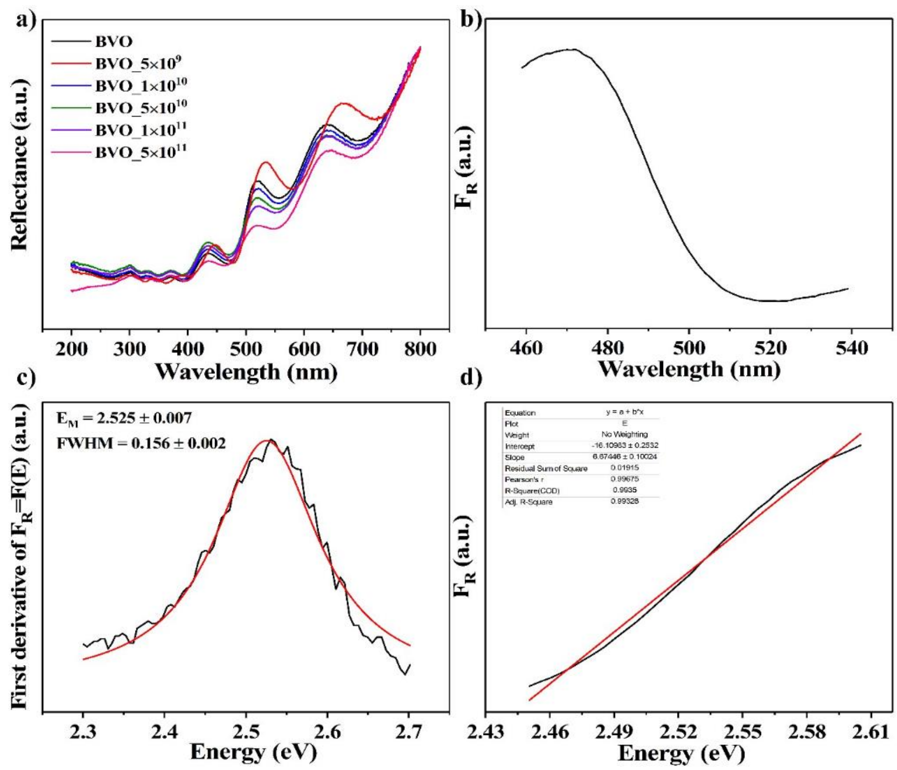

Fig. S2. a) DRS spectra of pristine and irradiated samples; b) Kubelka-Munk transformation of reflectance obtained from DRS for the pristine BVO; c) First derivative (black curve) and Voigt fit (red curve) of the $F_R = f(E)$ for the sample BVO. d) Linear fit (red curve) of the $F_R = f(E_i)$ (black curve) for the sample BVO.

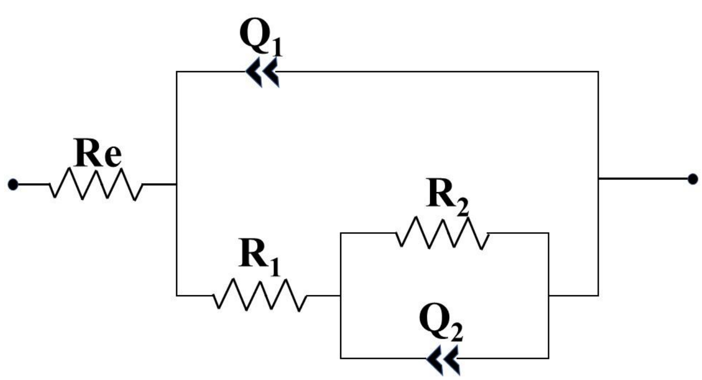

Fig. S3. Equivalent circuit (ECQ) model. The ECQ comprises several components: the series resistance Re, which encompasses the resistances of the FTO film, external electrical contacts, and the liquid electrolyte; the constant phase element (CPE), Q1, representing direct charge transfer at the semiconductor/electrolyte interface; the charge transfer resistance R1, signifying the trapping of charges in surface states; and the parallel combination of resistance R2 and CPE Q2, illustrating charge transfer between the electrolyte and surface states.

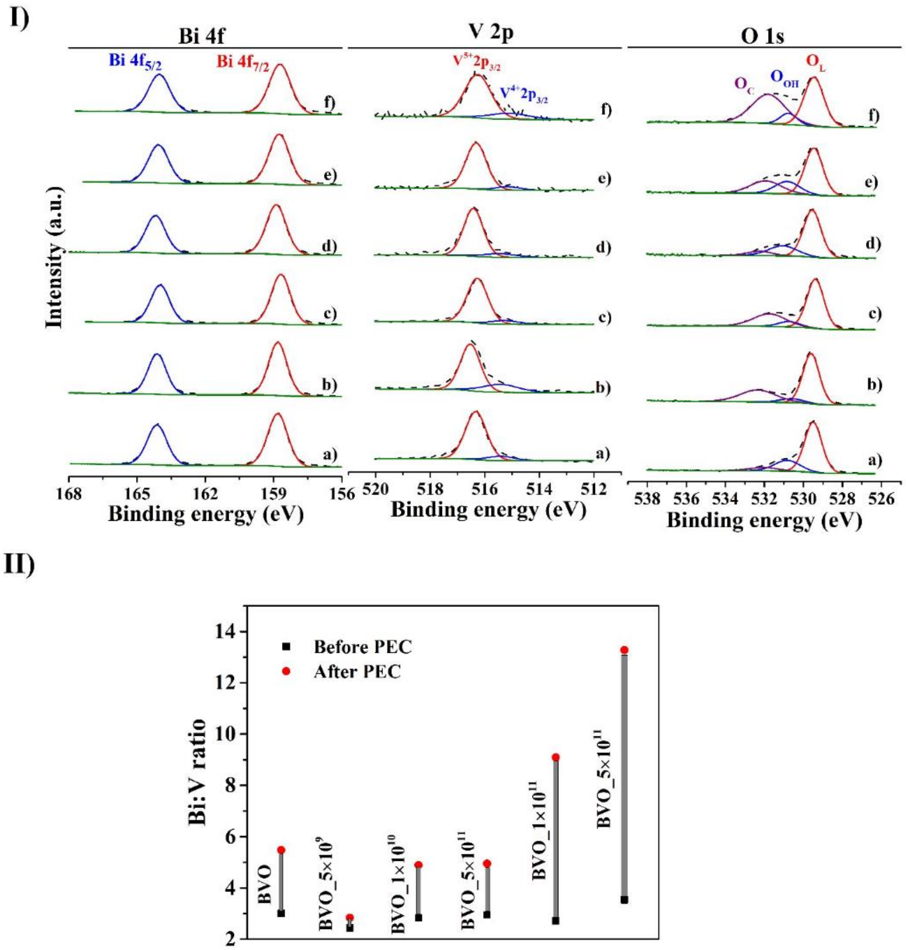

Fig. S4. I) XPS spectra of Bi 4f, V 2p and O 1s for a) BVO, b) BVO_5×10^9, c) BVO_1×10^{10}, d) BVO_5×10^{10}, e) BVO_1×10^{11} and f) BVO_5×10^{11} after PEC; II) Bi:V atomic ratio calculated by the integration of core-level signals before and after PEC.

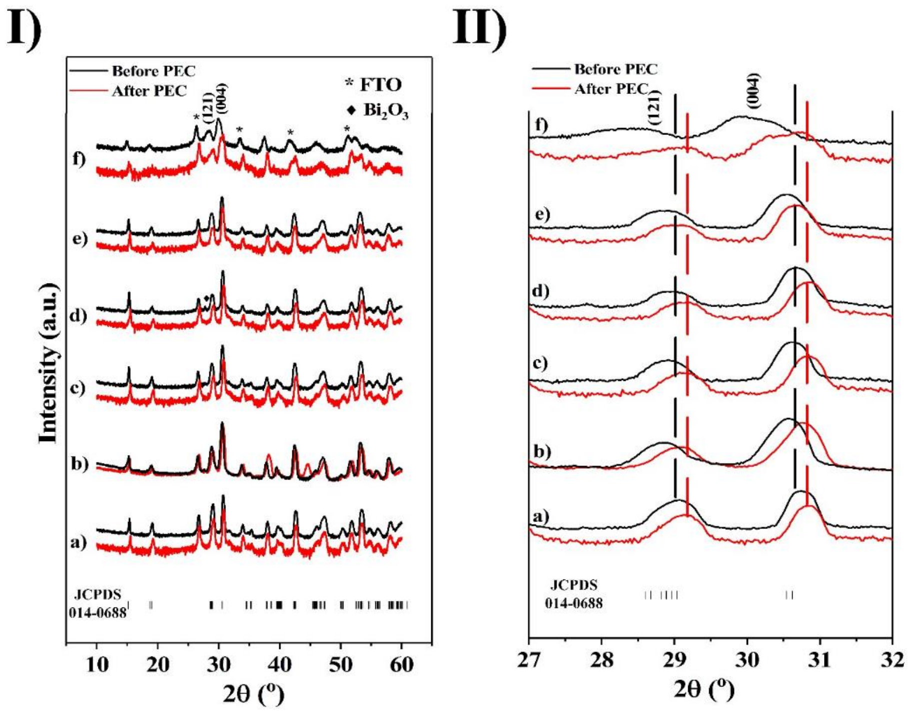

Fig. S5. I) Full and II) selectively magnified XRD patterns close to the (121) and (004) diffraction maxima of a) BVO, b) BVO_5×10^9, c) BVO_1×10^{10}, d) BVO_5×10^{10}, e) BVO_1×10^{11}, f) BVO_5×10^{11} before (black line) and after (red line) PEC;

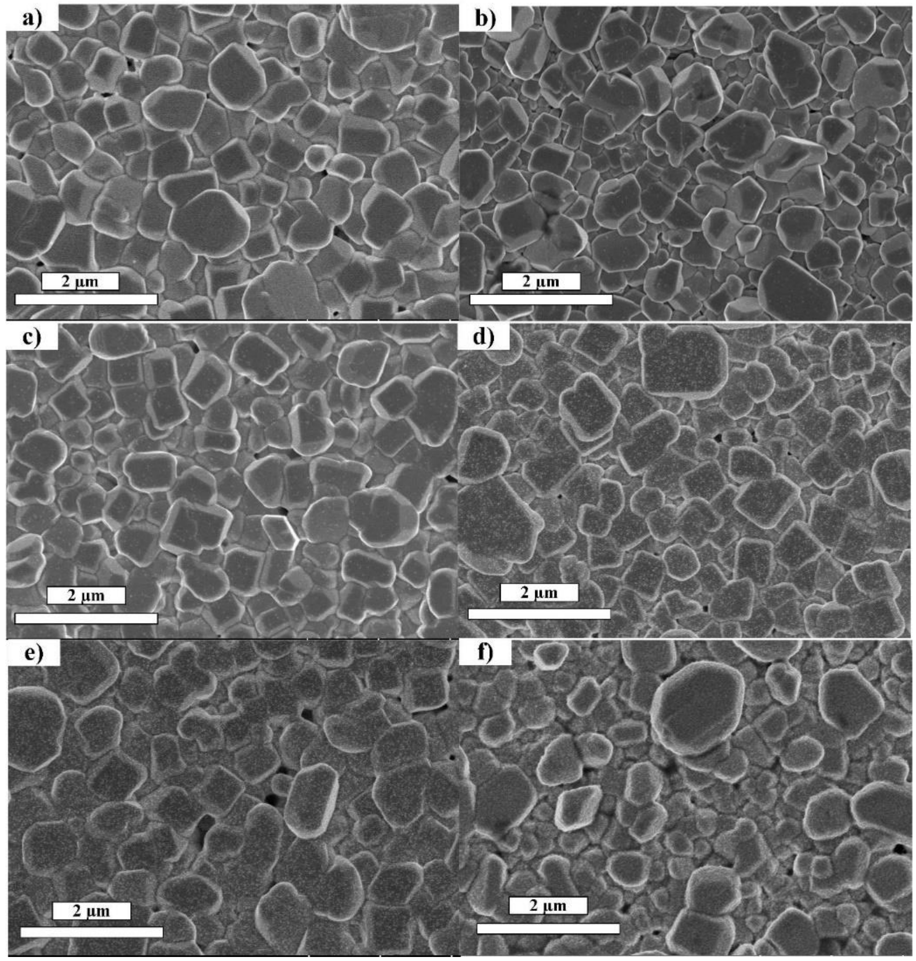

Fig. S6. SEM micrographs of a) BVO, b) BVO_5×10^9, c) BVO_1×10^{10}, d) BVO_5×10^{10}, e) BVO_1×10^{11}, f) BVO_5×10^{11} before PEC measurements.

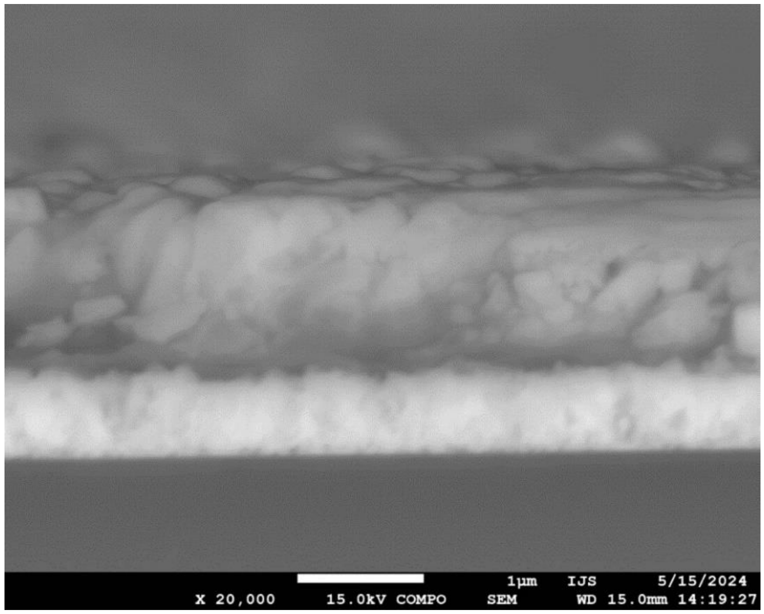

Fig. S7. Cross section of BVO film on FTO substrate

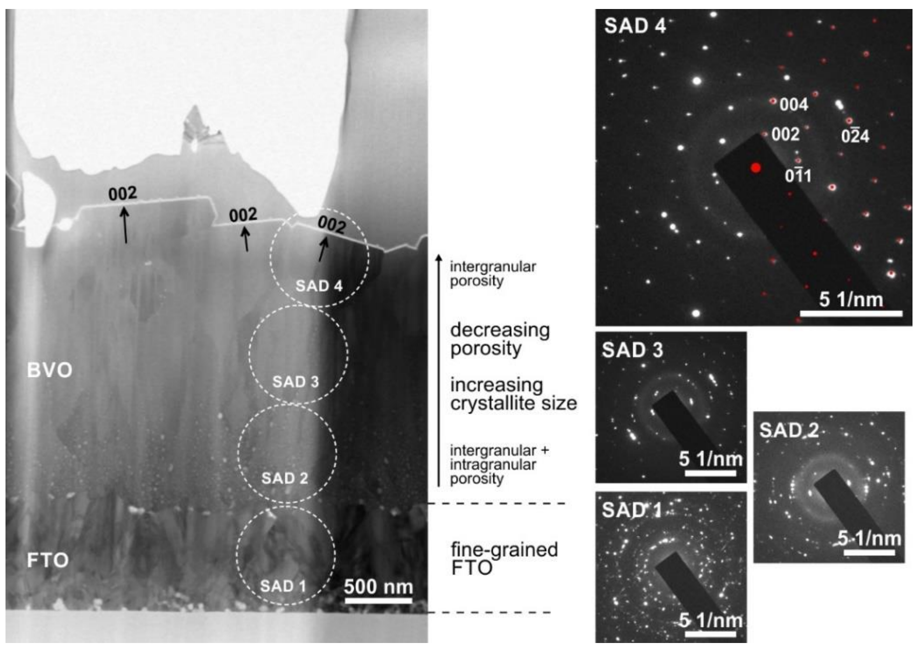

Fig. S8. SAD patterns recorded at various depths of the irradiated sample show that the FTO layer is fine-grained with random orientation of crystallites. BVO directly above contact with FTO is composed of smaller crystallites with many intragranular and intergranular pores. BVO crystallite size increases toward the surface and the upper crystallites are terminated by (002) lattice planes. These main microstructural characteristics are common to all three samples (*see* Fig. 4 in the main text).

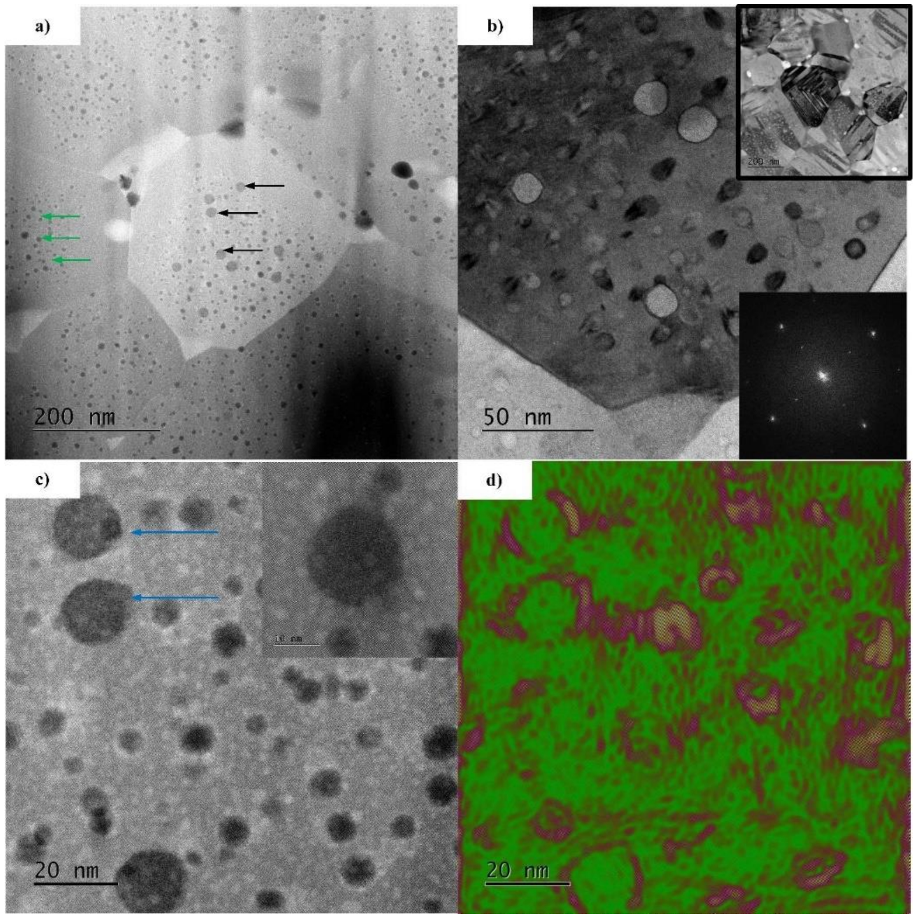

Fig. S9. Top-view morphological analysis of BVO_1×10^{10} representing the difference in nature of intragranular and intergranular voids with ion tracks; a) ADF and b) BF TEM with upper inset representing planar defects in the structure and lower inset representing faceted nature of intragranular voids; c) High-Angle Annular Dark-Field (HAADF) STEM with Moiré fringes in inset and d) Bragg-filtered image representing the overlap of ion tracks and intragranular voids.

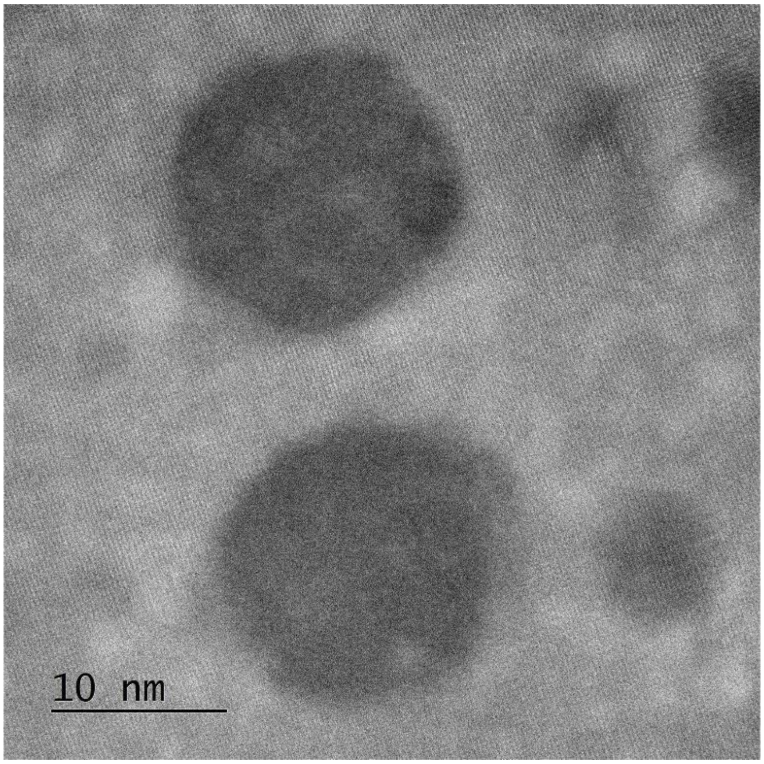

Fig. S10. Top-view STEM of ion-track in BVO_1×10^{10};

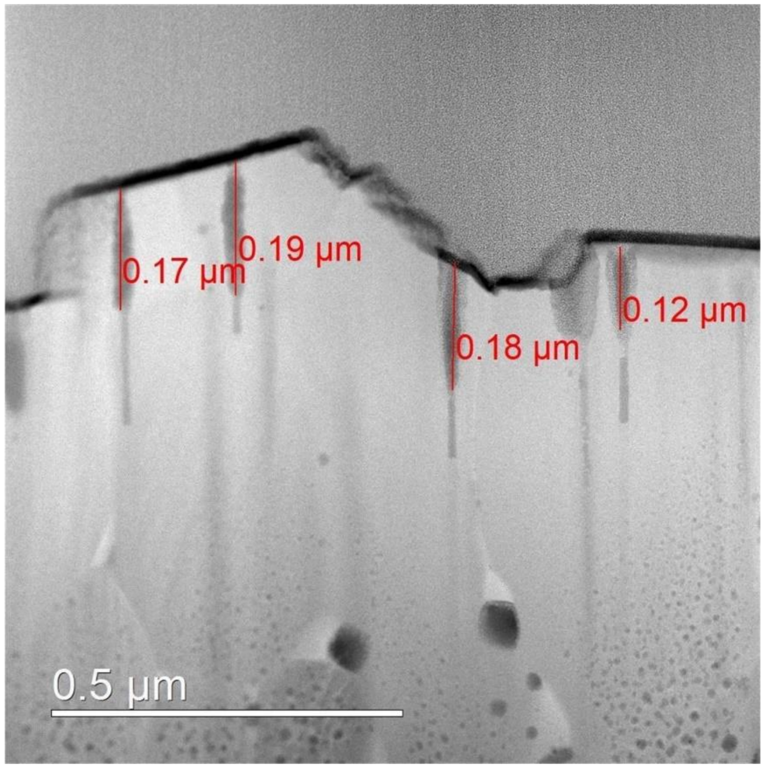

Fig. S11. STEM analysis of the BVO_1×10^{10} after PEC showing the variety in depth of the formed holes

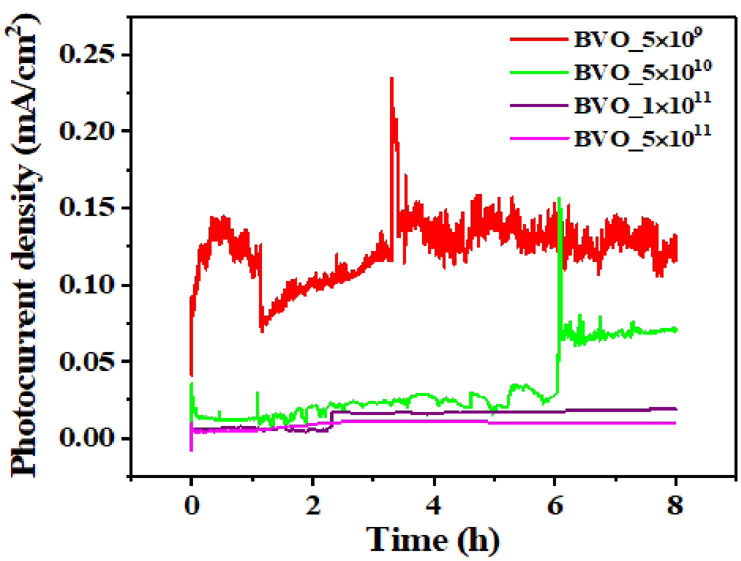

Fig. S12. 8-hour-long chronoamperometry in 0.1 M sodium borate buffer at 1.23 V *vs* RHE for BVO_5×10^9, BVO_5×10^{10}, BVO_1×10^{11} and BVO_5×10^{11};

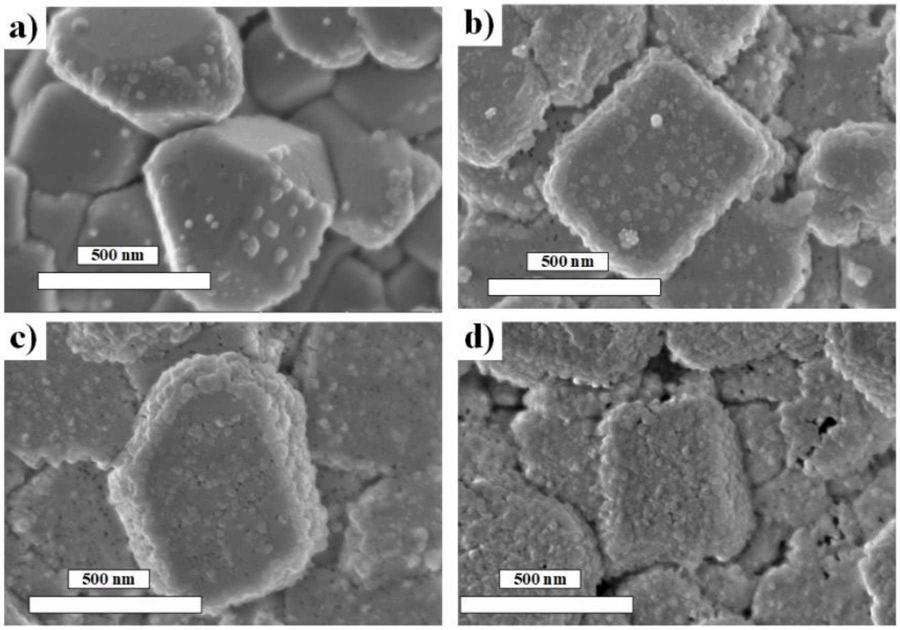

Fig. S13. SEM micrographs of a) BVO_5×10^9, b) BVO_5×10^{10}, c) BVO_1×10^{11} and d) BVO_5×10^{11}, respectively, after 8-hour-long chronoamperometry measurements.

Table S1. Atomic ratios calculated through the integration of its XPS core-level signals for pristine and irradiated samples before and after PEC

Sample	Bi:V	
	Before PEC	After PEC
BVO	3.00	5.48
BVO_5×10^{9}	2.44	2.84
BVO_1×10^{10}	2.84	4.89
BVO_5×10^{10}	2.95	4.95
BVO_1×10^{11}	3.54	9.09
BVO_5×10^{11}	2.72	13.28

Table S2. Literature survey of photocurrent densities at 1.23 V *vs.* RHE in undoped and uncatalyzed BVO in non-sacrificial electrolytes

Photocurrent density (mA/cm^2)	Reference
0.35	1
0.25	2
0.35	3
1.0	4
1.0	5
1.05	This work

Table S3. Parameters calculated from electrochemical impedance spectroscopy, Mott-Schottky impedance spectroscopy, and open-circuit potential measurements

Sample	Re (Ω)	R_1 (Ω)	R_2 (Ω)	N_D . 10^{20} (m^{-3})	Vph (mV)
BVO	149.7	54.8	303.1	6.56	181
BVO_5×10^9	147.5	48.9	863.5	1.22	130
BVO_1×10^{10}	92.8	28.4	390.3	2.11	312
BVO_5×10^{10}	100.1	49.5	1320	0.71	103
BVO_1×10^{11}	92.6	90.9	3900	0.42	60
BVO_5×10^{11}	90.7	94.8	132.8	0.14	6

References

1. C. W. Kim, Y. S. Son, M. J. Kang, D. Y. Kim, Y. S. Kang, *Adv. Energy Mater.* 2015, 6, 1501754.
2. S. Wang, P. Chen, J. H. Yun, Y. Hu, L. Wang, *Angew. Chem. Int. Ed. Engl.* 2017, 56, 8500.
3. G. Fang, Z. Liu, C. Han, *Appl. Surf. Sci.* 2020, 515, 146095.
4. X. Chen, C. Zhen, N. Li, N. Jia, X. Xu, L. Wang, G. Liu, *Small Methods* 2023, 7, 2201611.
5. B. J. Trzesniewski, I. A. Digdaya, T. Nagaki, S. Ravishankar, I. Herriaz-Cardona, D. A. Vermaas, A. Longo, S. Gimenez, W. A. Smith, *Energy Environ. Sci.* 2017,10, 1517.